J|A|C|S
ARTICLES
Published on Web 06/09/2004

Selective Reductive Desorption of a SAM-Coated Gold Electrode Revealed Using Fluorescence Microscopy

Jeff L. Shepherd,[†] Arnold Kell,[§] Emily Chung,[†] Chad W. Sinclair,[‡] Mark S. Workentin,[§] and Dan Bizzotto*,[†]

Contribution from the Department of Chemistry, Advanced Materials & Process Engineering Laboratory (AMPEL), University of British Columbia, Vancouver, BC, Canada, Department of Metals & Materials, Advanced Materials & Process Engineering Laboratory (AMPEL), University of British Columbia, Vancouver, BC, Canada, and Department of Chemistry, University of Western Ontario, London, ON, Canada

Received February 2, 2004; E-mail: bizzotto@chem.ubc.ca

Abstract: The reductive desorption of a self-assembled monolayer (SAM) of a fluorescent thiol molecule (BodipyC10SH) from Au was characterized using electrochemistry and epi-fluorescence microscopy. Molecular luminescence is quenched near a metal surface, so fluorescence was only observed for molecules reductively desorbed and then separated from the electrode surface. Fluorescence imaging showed that reductive desorption was selective, with desorption occurring from different regions of the Au electrode depending on the extent of the negative potential excursion. When desorbed, the molecules were sufficiently mobile, diffusing away from the electrode surface, thereby preventing oxidative readsorption. At sufficiently negative desorption potentials, all of the thiol was desorbed from the electrode surface, resulting in fluorescence at the air/solution interface. The selective removal of the thiol monolayer from distinct regions was correlated to features on the electrode surface and was explained through potential-dependent interfacial energies. This in situ electrofluorescence microscopy technique may be useful in sensor development.

1. Introduction

The functionalization of metal surfaces by adsorbed organic molecules is a rapidly expanding area of science because of its potential application in sensors and in nanotechnology.[1−8] The most common organic-modified metal cited involves the formation of a robust self-assembled monolayer (SAM) of thiol molecules on noble metals, most notably Au.[9] With the ease of forming such an interface, it has proven to be a popular subject for the creation of an ideal environment for the study of chemically tunable surfaces,[10−12] and thus the reproducibility of the monolayer has become the subject of much discussion.[13−17] Physically adsorbed organic molecules are also a viable, but frequently overlooked candidate for the modification of surfaces for device applications. In either case, the engineering of such devices based on surface modification is hampered by our limited understanding of nanoscale physical and chemical processes such as adsorption and desorption of a surfactant. Therefore, a better understanding of the universal properties of adsorbed surfactants ranging from chemisorbed to physisorbed will give us access to a wider range of exploitable properties.

Various probes have been employed to characterize the quality of adsorbed surfactants including electrochemical techniques, which through the control of interfacial energetics can result in conformational changes and/or desorption of the organic from the metal. The process of adsorption/desorption has been observed to be very reproducible for physisorbed organic molecules on Au(111) and Hg electrode surfaces in neutral electrolyte.[18] In the case of the thiol SAM, very negative potentials are required for reductive desorption, and therefore to circumvent hydrogen evolution a strongly alkaline electrolyte is required.[19−52] The readsorption of the thiol can occur through

[†] Department of Chemistry, University of British Columbia.
[‡] Department of Metals & Materials, University of British Columbia.
[§] University of Western Ontario.

(1) Ishida, T. *Springer Ser. Chem. Phys.* **2003**, *70*, 91−106.
(2) Schwartz, D. K. *Annu. Rev. Phys. Chem.* **2001**, *52*, 107−137.
(3) Brockman, J. M.; Nelson, B. P.; Corn, R. M. *Annu. Rev. Phys. Chem.* **2000**, *51*, 41−63.
(4) Ulman, A.; Kang, J. F.; Shnidman, Y.; Liao, S.; Jordan, R.; Choi, G.-Y.; Zaccaro, J.; Myerson, A. S.; Rafailovich, M.; Sokolov, J.; Fleischer, C. *Rev. Mol. Biotechnol.* **2000**, *74*, 175−188.
(5) Badia, A.; Lennox, R. B.; Reven, L. *Acc. Chem. Res.* **2000**, *33*, 475−481.
(6) Ulman, A. *Chem. Rev.* **1996**, *96*, 1533−1554.
(7) Honeychurch, M. J. *Recent Res. Dev. Electroanal. Chem.* **2000**, *2*, 1−16.
(8) Everhart, D. S. *Handb. Appl. Surf. Colloid Chem.* **2002**, *2*, 99−116.
(9) Bard, A.; Abruna, H. D.; Chidsey, C.; Faulkner, L. R.; Feldberg, S. W.; Itaya, K.; Majda, M.; Melroy, O.; Murray, R. W.; Porter, M. D.; Soriaga, M. P.; White, H. S. *J. Phys. Chem.* **1993**, *97*, 7147.
(10) Penn, S. G.; He, L.; Natan, M. J. *Curr. Opin. Chem. Biol.* **2003**, *7*, 609−615.
(11) Battaglini, N.; Klein, H.; Dumas, P.; Moustrou, C.; Samat, A. *Appl. Surf. Sci.* **2003**, *212*−*213*, 481−484.
(12) Sinner, E.-K.; Knoll, W. *Curr. Opin. Chem. Biol.* **2001**, *5*, 705−711.
(13) Badia, A.; Back, R.; Lennox, R. B. *Angew. Chem., Int. Ed. Engl.* **1994**, *33*, 2332.
(14) Boubour, E.; Lennox, R. B. *J. Phys. Chem. B* **2000**, *104*, 9004−9010.
(15) Boubour, E.; Lennox, R. B. *Langmuir* **2000**, *16*, 7464−7470.
(16) Ma, F.; Lennox, R. B. *Langmuir* **2000**, *16*, 6188−6190.
(17) Boubour, E.; Lennox, R. B. *Langmuir* **2000**, *16*, 4222−4228.
(18) Bizzotto, D.; Yang, Y.; Shepherd, J. L.; Stoodley, R.; Agak, J. O.; Stauffer, V.; Lathuilliere, M.; Ahktar, A.; Chung, E. *J. Electroanal. Chem.* **2004**.
(19) Walczak, M. M.; Popenoe, D. D.; Deinhammer, R. S.; Lamp, B. D.; Chung, C.; Porter, M. D. *Langmuir* **1991**, *7*, 2687−2693.
(20) Widrig, C. A.; Chung, C.; Porter, M. D. *J. Electroanal. Chem.* **1991**, *310*, 335−359.
(21) Weisshaar, D. E.; Lamp, B. D.; Porter, M. D. *J. Am. Chem. Soc.* **1992**, *114*, 5860−5862.

an oxidative process; however, this is strongly dependent on the length of the alkyl chain comprising the thiol. Completely irreversible desorption has been observed for short alkyl chain thiols ($n = 2-8$), while a reversible process was noted for thiols of longer alkyl chains ($n > 16$).[30,32,33,53] Furthermore, experiments using single-crystal electrodes have shown that this reductive desorption process is dependent on crystallographic orientation and on the length of the alkyl chain.[25,28,30] This dependence on surface crystallography has also been observed for the physically adsorbed surfactants.[54] Morin has completed a series of studies illuminating this process based upon electrochemical and in situ FTIR studies.[26,31,34,41] Reductive desorption has also been imaged with in situ STM.[39,45,52,55-58] In all of these studies, the fate of the desorbed molecules is not clearly understood and has only been indirectly experimentally observed.

Sometimes a multifunctional or patterned surface with more than one type of chemical functionality is required and has led to the investigation of thiol exchange reactions where more weakly bound thiols are replaced by a stronger interacting thiol from solution.[39,59,60] The search continues for more flexible types of chemical patterning, and the selective removal of surfactant from certain areas of the surface offers one possibility. This method of removing the bound thiol has been used to create a multiple component thiol layer by reductively desorbing a portion of the original SAM, and then allowing another thiol molecule to assemble into these void spaces;[29,36,39,46,47,57,61] however, achieving this with a desired pattern is difficult. Reductive desorption of a thiol SAM from metals of low index surfaces has been observed to occur at reasonably separated cathodic potentials.[28,62] Thus, an ideally shaped nanocrystal in a truncated octahedron geometry containing both the (111) and the (100) surfaces may be exploited in creating a patterned surface by the selective removal of thiol from one face. The ability to selectively desorb certain regions of the thiol will be examined in this report using a multifaceted substrate.

To fully characterize this process, we will combine electrochemical techniques with a recently developed in situ probe. As mentioned earlier, electrochemical methods allow us to control the properties of a modified electrode. Coupling electrochemistry with in situ techniques can enable observation of the direct response to potential perturbations. While fluorescence is widely used in the microscale characterization of biological systems, it has been underutilized at this scale for the study of physical and chemical phenomena. Recent spatially resolved observations of electrochemically induced changes in an adsorbed monolayer[63,64] using epi-fluorescence microscopy demonstrate its versatility in the characterization of interfaces. This fluorescence technique is useful because molecular luminescence near metal surfaces is strongly related to the distance separating the fluorophore from the metal. At close proximity (<50 nm), fluorescence is efficiently quenched by nonradiative energy transfer into surface plasmons and electron hole pairs in the metal.[65,66] Therefore, fluorescence will only be observed if the desorbed molecule is far from the metal surface. Thus, the reductive desorption of a fluorescent thiol monitored by this technique will result in an understanding of the desorption process and fate of desorbed thiolates. By employing a multifaceted metal substrate, the selective reductive desorption will be illuminated at different potentials due to the different energetics of each face. We describe such a process by monitoring the potential-induced desorption of a fluorescent-labeled thiol from various facets of a polycrystalline Au bead. Selective desorption from specific regions of the electrode surface, controlled by potential, will be demonstrated, and the fate of these desorbed molecules will be monitored. Finally, we will link these results on the thiol SAM with the previously published work on the electrochemical and spectroelectrochemical characterization of physically adsorbed monolayers to reveal some similarities between the two. The ability to selectively desorb the thiol from certain facets of the metal surface is

(22) Weisshaar, D. E.; Walczak, M. M.; Porter, M. D. *Langmuir* **1993**, *9*, 323−329.
(23) Schneider, T. W.; Buttry, D. A. *J. Am. Chem. Soc.* **1993**, *115*, 12391−12397.
(24) Abbott, N. L.; Gorman, C. B.; Whitesides, G. M. *Langmuir* **1995**, *11*, 16−18.
(25) Yang, D. F.; Wilde, C. P.; Morin, M. *Langmuir* **1996**, *12*, 6570−6577.
(26) Yang, D. F.; Morin, M. *J. Electroanal. Chem.* **1997**, *429*, 1−5.
(27) Finklea, H. O. *Electroanal. Chem.* **1996**, *19*, 109−335.
(28) Zhong, C.-J.; Zak, J.; Porter, M. D. *J. Electroanal. Chem.* **1997**, *421*, 9−13.
(29) Imabayashi, S.; Hobara, D.; Kakiuchi, T.; Knoll, W. *Langmuir* **1997**, *13*, 4502−4504.
(30) Zhong, C.-J.; Porter, M. D. *J. Electroanal. Chem.* **1997**, *425*, 147−153.
(31) Yang, D. F.; Al-Maznai, H.; Morin, M. *J. Phys. Chem. B* **1997**, *101*, 1158−1166.
(32) Yang, D. F.; Wilde, C. P.; Morin, M. *Langmuir* **1997**, *13*, 243−249.
(33) Yang, D. F.; Morin, M. *J. Electroanal. Chem.* **1998**, *441*, 173−181.
(34) Byloos, M.; Al-Maznai, H.; Morin, M. *J. Phys. Chem. B* **1999**, *103*, 6554−6561.
(35) Badia, A.; Arnold, S.; Scheumann, V.; Zizlsperger, M.; Mack, J.; Jung, G.; Knoll, W. *Sens. Actuators, B* **1999**, *B54*, 145−165.
(36) Kuwabata, S.; Kanemoto, H.; Oyamatsu, D.; Yoneyama, H. *Electrochemistry (Tokyo)* **1999**, *67*, 1254−1257.
(37) Kawaguchi, T.; Yasuda, H.; Shimazu, K.; Porter, M. D. *Langmuir* **2000**, *16*, 9830−9840.
(38) Wong, S.-S.; Porter, M. D. *J. Electroanal. Chem.* **2000**, *485*, 135−143.
(39) Kakiuchi, T.; Sato, K.; Iida, M.; Hobara, D.; Imabayashi, S.; Niki, K. *Langmuir* **2000**, *16*, 7238−7244.
(40) Calvente, J. J.; Andreu, R.; Gil, M.-L. A.; Gonzalez, L.; Alcudia, A.; Dominguez, M. *J. Electroanal. Chem.* **2000**, *482*, 18−31.
(41) Byloos, M.; Al-Maznai, H.; Morin, M. *J. Phys. Chem. B* **2001**, *105*, 5900−5905.
(42) Mulder, W. H.; Calvente, J. J.; Andreu, R. *Langmuir* **2001**, *17*, 3273−3280.
(43) Imabayashi, S.; Hobara, D.; Kakiuchi, T. *Langmuir* **2001**, *17*, 2560−2563.
(44) Esplandiu, M. J.; Hagenstroem, H.; Kolb, D. M. *Langmuir* **2001**, *17*, 828−838.
(45) Wano, H.; Uosaki, K. *Langmuir* **2001**, *17*, 8224−8228.
(46) Satjapipat, M.; Sanedrin, R.; Zhou, F. *Langmuir* **2001**, *17*, 7637−7644.
(47) Oyamatsu, D.; Kanemoto, H.; Kuwabata, S.; Yoneyama, H. *J. Electroanal. Chem.* **2001**, *497*, 97−105.
(48) Byloos, M.; Rifai, S.; Al-Maznai, H.; Laferriere, M.; Morin, M. *Langmuir* **2001**, *17*, 2478−2484.
(49) Kakiuchi, T.; Usui, H.; Hobara, D.; Yamamoto, M. *Langmuir* **2002**, *18*, 5231−5238.
(50) Plummer, S. T.; Bohn, P. W. *Langmuir* **2002**, *18*, 4142−4149.
(51) Brask, J.; Wackerbarth, H.; Jensen, K. J.; Zhang, J.; Chorkendorff, I.; Ulstrup, J. *J. Am. Chem. Soc.* **2003**, *125*, 94−104.
(52) Loglio, F.; Schweizer, M.; Kolb, D. M. *Langmuir* **2003**, *19*, 830−834.
(53) Aoki, K.; Kakiuchi, T. *J. Electroanal. Chem.* **1998**, *452*, 187−192.
(54) Bizzotto, D.; Noeel, J. J.; Lipkowski, J. *Thin Solid Films* **1994**, *248*, 69−77.
(55) Hobara, D.; Miyake, K.; Imabayashi, S.; Niki, K.; Kakiuchi, T. *Langmuir* **1998**, *14*, 3590−3596.
(56) Schneeweiss, M. A.; Hagenstrom, H.; Esplandiu, M. J.; Kolb, D. M. *Appl. Phys. A* **1999**, *69*, 537−551.
(57) Hobara, D.; Sasaki, T.; Imabayashi, S.; Kakiuchi, T. *Langmuir* **1999**, *15*, 5073−5078.
(58) Dunbar, T. D.; Cygan, M. T.; Bumm, L. A.; McCarty, G. S.; Burgin, T. P.; Reinerth, W. A.; Jones, L.; Jackiw, J. J.; Tour, J. M.; Weiss, P. S.; Allara, D. L. *J. Phys. Chem. B* **2000**, *104*, 4880−4893.
(59) Felgenhauer, T.; Rong, H.-T.; Buck, M. *J. Electroanal. Chem.* **2003**, *550−551*, 309−319.
(60) Chung, C.; Lee, M. *J. Electroanal. Chem.* **1999**, *468*, 91−97.
(61) Shimazu, K.; Kawaguchi, T.; Isomura, T. *J. Am. Chem. Soc.* **2002**, *124*, 652−661.
(62) Walczak, M. M.; Alves, C. A.; Lamp, B. D.; Porter, M. D. *J. Electroanal. Chem.* **1995**, *396*, 103−114.
(63) Shepherd, J.; Yang, Y.; Bizzotto, D. *J. Electroanal. Chem.* **2002**, *524−525*, 54−61.
(64) Shepherd, J. L.; Bizzotto, D. *J. Phys. Chem. B* **2003**, *107*, 8524−8531.
(65) Pineda, A. C.; Ronis, D. *J. Chem. Phys.* **1985**, *83*, 5330−5337.
(66) Chance, R. R.; Prock, A.; Silbey, R. In *Advances in Chemical Physics*; Prigogine, I., Ed.; Interscience Publishers: New York, 1978; Vol. 37, pp 1−65.

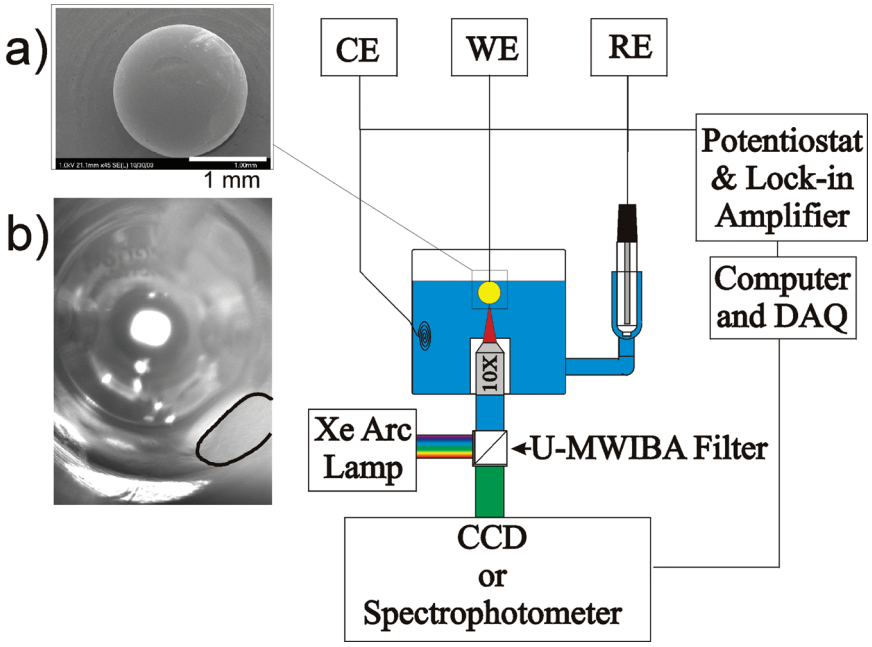

Figure 1. Schematic representation of the epi-fluorescence setup used for imaging during electrochemical measurements. (a) SEM of the bead electrode; (b) brightfield image of the bead electrode taken just before fluorescence measurements; the facet located on the bottom right is outlined.

Scheme 1. The Synthesis of BiodipyC10SH

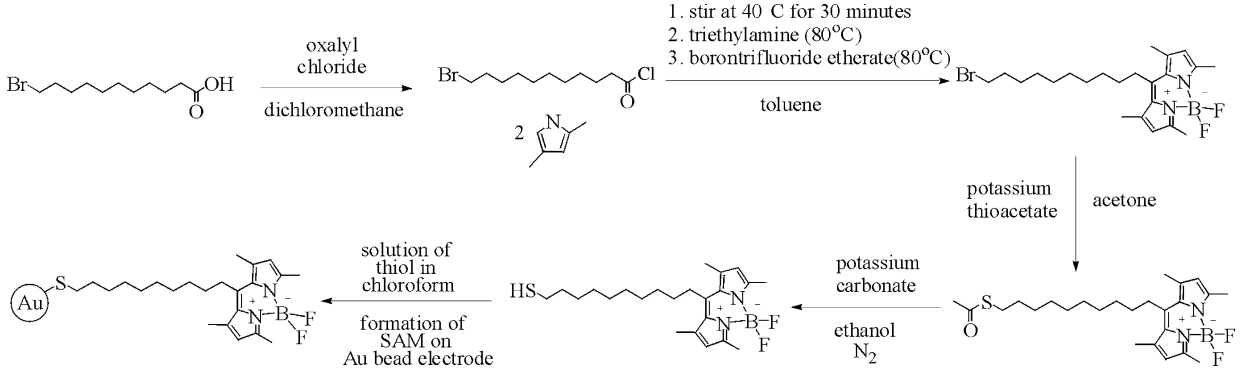

attributed to the electric variable having control over the tension of each face (electrocapillarity).

2. Experimental Section

2.1. Synthesis of BodipyC10SH. The fluorophore thiol precursor utilized as the probe in this study, 4,4-difluoro-1,3,5,7-tetramethyl-8-[(10-mercapto)]-4-bora-3a,4a-diaza-*s*-indacene (BodipyC10SH), was synthesized using the procedure outlined in Scheme 1. Full experimental and characterization details are provided in the Supporting Information.

2.2. Electrochemistry. Electrochemical investigations were performed on an electropolished Au bead working electrode (SEM image shown in Figure 1a), a Au coil counter electrode, and a saturated calomel (SCE) reference electrode connected to the working solution through a salt bridge. The 0.1 M NaOH supporting electrolyte (Fluka, suprapur used as received) was prepared in Millipore water (>18 MΩ cm) and purged with Ar (Praxair, cleaned with a charcoal filter, Supelco). A constant blanket of Ar was maintained above the electrolyte throughout the experiment. Solution cleanliness was confirmed by cyclic voltammetry (CV) and differential capacitance measurements of the Au bead in NaOH electrolyte prior to the surface modification. The SAM was formed by introducing the clean, dry bead into a solution of dissolved thiol in chloroform (3 mg/mL) for roughly 10 min. The bead was then rinsed with water, followed by sonication in a methanol solution to remove the physically adsorbed thiol. After evaporation of methanol, the SAM-coated electrode was introduced to the electrolyte and positioned just above the microscope objective port (see Figure 1) in an arrangement suitable for in situ investigation.

2.3. Electron Backscattered Diffraction (EBSD). EBSD[67] was used to determine the crystallographic surface normal for various regions of the Au electrode. Indexing of the backscattered Kikuchi pattern was performed via an automated software algorithm (HKL Channel 5 software). Measurement of the crystallographic surface normal necessitates that the facet be precisely tilted within the microscope such that each facet faces the detector and is at 70° to the horizontal plane. While this technique has previously been used for the study of faceted surfaces,[68] the difficulty in precisely aligning each of the facets decreases the accuracy of the technique. The magnitude of this error was judged by measuring the known surface normal for a series of Si single crystals mounted such that they were oriented at random angles to the horizontal. It was found that the error in manually positioning the facets to 70° within the microscope introduced an error of no more than ±10° in the measured crystallographic surface normal. While this error is large relative to the normal systematic error involved in EBSD measurements (~1−2°), it was felt to be sufficient for the current study.

2.4. Spectroelectrochemistry.

2.4.1. Epi-fluorescence Imaging. Fluorescence imaging was performed on an Olympus IX70 inverted microscope equipped with a 10×

(67) Randle, V.; Engler, O. *Introduction to Texture Analysis*; Gordon and Breach: Amsterdam, 2000.
(68) Davies, P. A.; Randle, V. *J. Microsc.* **2001**, *204*, 29−38.

objective (NA = 0.3, wd = 10 mm) and a SPOT RT digital camera. The inverted arrangement enabled looking up onto the surface of the working electrode as shown in Figure 1. SEM and brightfield images of the electrode are shown. All images of fluorescence reported were collected using a Xe arc lamp and a U-MWIBA filter cube (Olympus: BP 460, DM 505, BA 515lF), resulting in images of roughly 1 × 1.5 mm with a resolution of 1.93 μm/pixel (2 × 2 binning, 8 bit). Each image was acquired with an exposure time of 50 ms and a gain of 1.

One potential step-imaging cycle consisted of a series of potential steps. Starting at 0 mV/SCE, the potential was incrementally stepped ($\Delta E = -50$ mV) to a predetermined negative potential, and then the potential was stepped back to 0 mV/SCE ($\Delta E = 50$ mV). After every step, interfacial capacitance and fluorescence images were recorded. The potential steps were separated by 2 s, resulting in a scan rate of roughly 25 mV/s. These potential-imaging cycles were applied to the modified Au bead electrode with each successive cycle employing a more negative turn-around potential (−0.950, −1.250, −1.300, −1.350, and −1.400 V/SCE). In addition, once reaching the negative potential of each cycle, the potential was held for 6 s to allow for acquisition of three images and capacitance. Before each potential step-imaging cycling procedure, one CV cycle using the same negative potential limit was recorded (20 mV/s).

2.4.2. Image Analysis. All images were analyzed using dip_image[69] for MATLAB and Image Pro Plus 4.5. The average gray scale, which was assumed to be proportional to the fluorescence intensity, was calculated using a MATLAB procedure after subtracting the 0 mV/SCE fluorescence image (to correct for the small background due to scattered light).

3. Results and Discussion

3.1. Electrochemical and Epi-fluorescence Investigations. The BodipyC10SH-modified gold bead electrode was introduced to the electrochemical cell at $E = 0$ V/SCE. The stability of the SAM was first probed in a limited potential range using cyclic voltammetry (CV) prior to fluorescence imaging and capacitance measurement. To ensure that the fluorescent headgroup remained stable, the measurements were conducted in less basic pH conditions than those typically used for reductive desorption studies of alkanethiols. Therefore, the reductive desorption peak reported in these studies would have been obscured by hydrogen evolution at this lower pH. Capacitive measurements will be presented because we are primarily interested in these changes that are more sensitive and reliable than the currents measured in CV. Figures 2 and 3 show results for concurrent measurements of capacitance and fluorescence during each potential-imaging cycle. A selection of fluorescence images are shown in Figure 4, which correspond to the letter legend in Figure 3. It is important to reinforce that the same SAM-coated surface was probed using a series of capacitance and fluorescence experiments with a progressively more negative potential limit.

A freshly modified electrode surface immersed at $E = 0$ V/SCE had a capacitance which was much lower (1.2 μF cm^{-2}) than the uncoated electrode surface, demonstrating the formation of a well-ordered layer SAM despite the bulky headgroup and short assembly time (10 min). Longer assembly times (>20 h) were not used because the minimum capacitance did not significantly change and presumably a less organized layer would be more responsive to potential, and less influenced by other effects (e.g., strong hydrophobic intermolecular interactions). Fluorescence from the electrode was recorded, and the

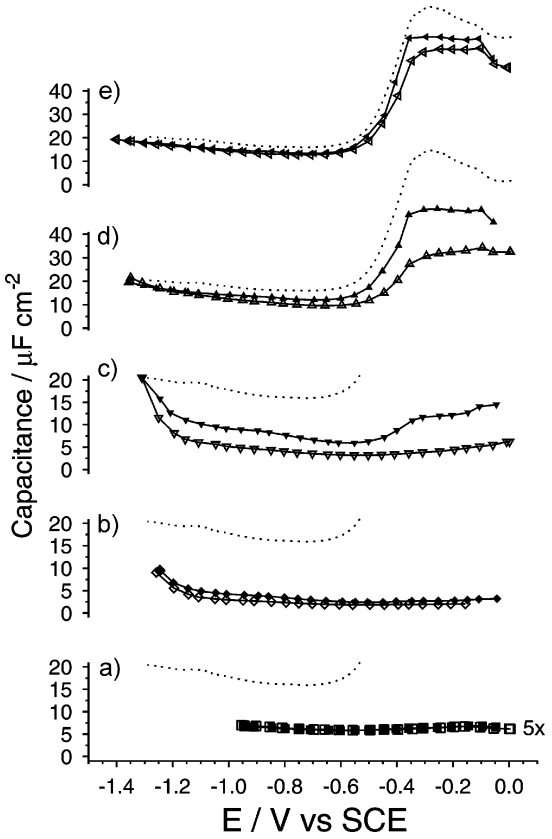

Figure 2. Capacitance measured during fluorescence imaging for the same modified electrode surface with a sequentially changing negative potential limit starting from (a) −0.950, (b) −1.250, (c) −1.300, (d) −1.350, and (e) −1.400 V/SCE. The dotted line represents the capacitance scan measured for the bare Au electrode in contact with 0.1 M NaOH. Positive going (closed symbols) and negative going scans (open symbols) for the modified electrode are also shown. Capacitance is calculated assuming a series RC circuit, 25 Hz, 5 mV rms.

capacitance was measured as the potential was stepped in a negative direction in 50 mV intervals from the initial potential to the first negative potential limit of −0.950 V/SCE. At this negative potential, three fluorescence images were acquired. The potential was then stepped positively in 50 mV increments back to the initial potential. A small increase in the capacitance at the positive limit was observed after one potential cycle, suggesting some disruption or disorder of the SAM. The corresponding fluorescence measurements show a small increase in the fluorescence at the negative potential limit. This potential-dependent fluorescence was used in the study of physically adsorbed surfactants on gold electrodes[63,70,71] as well as by Gaigalas in the study of the dynamics of immobilized fluorophores[72,73] and fluorescein-labeled single-strand oligonucleotides immobilized onto gold.[74] The changes in fluorescence are due to a slight increase in the distance between the fluorophore and the electrode surface. The increase in interfacial capacitance suggests a partial desorption of some thiol, with the desorbed molecules moving away from the interface.

(69) van Vliet, L. J. DIPLib, the Delft Image Processing Library; http://www.ph.tn.tudelft.nl/DIPLib/DIPLib.html.

(70) Bizzotto, D.; Lipkowski, J. *J. Electroanal. Chem.* **1996**, *409*, 33−43.
(71) Sagara, T.; Zamlynny, V.; Bizzotto, D.; McAlees, A.; McCrindle, R.; Lipkowski, J. *Isr. J. Chem.* **1997**, *37*, 197−211.
(72) Gaigalas, A. K.; Li, L.; Ruzgas, T. *Curr. Top. Colloid Interface Sci.* **1999**, *3*, 83−101.
(73) Li, L.; Meuse, C.; Silin, V.; Gaigalas, A. K.; Zhang, Y. *Langmuir* **2000**, *16*, 4672−4677.
(74) Wang, L.; Silin, V.; Gaigalas, A. K.; Xia, J.; Gebeyehu, G. *J. Colloid Interface Sci.* **2002**, *248*, 404−412.

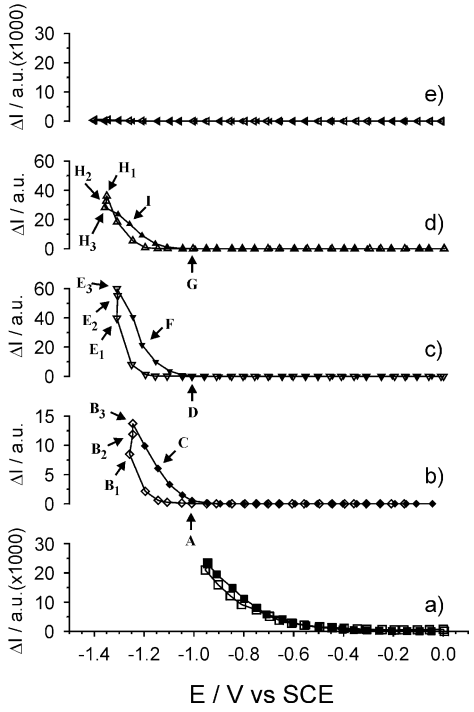

Figure 3. Potential-dependent average fluorescence intensity measured from the same electrode surface with sequentially changing negative potential limit starting at (a) −0.950, (b) −1.250, (c) −1.300, (d) −1.350, and (e) −1.400 V/SCE. Positive (open symbols) and negative potential scans (closed symbols) are also shown.

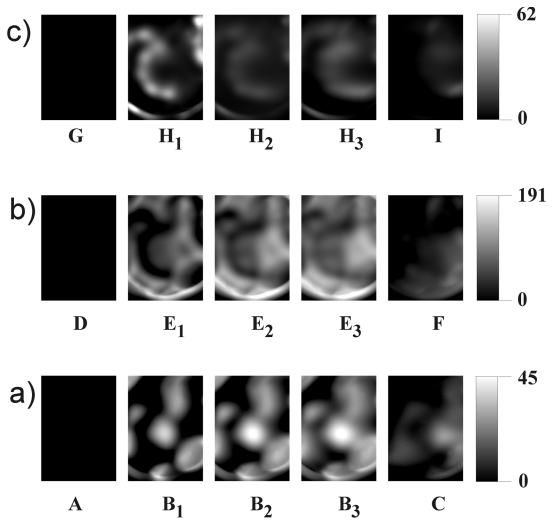

Figure 4. Fluorescence images from the same electrode for various potentials (letters correspond to potentials and intensities shown in Figure 3) obtained during potential scans to differing negative potentials: (a) −1.250, (b) −1.300, (c) −1.350V/SCE.

The negative limit for the subsequent potential scan was made more negative (−1.250 V/SCE), resulting in a significant increase in capacitance demonstrating the instability of the monolayer toward large negative potentials. The minimum capacitance of the SAM-coated interface has increased to 3 μF cm^{-2} (measured at the positive potential limit). At the negative potential limit, the capacitance increased strongly, indicating the penetration of the SAM by the electrolyte through potential created defects in the layer caused by the initial stages of reductive desorption. The change in capacitance at this potential was accompanied by a marked increase in the average fluorescence intensity, also consistent with significant reductive desorption at this potential. Some surfactant was desorbed from the metal surface, and, for fluorescence to be observed, this surfactant must be separated from the metal by some as yet undetermined distance.

These results for the desorption of a SAM exactly parallel the results previously published for the desorption of physically adsorbed lipid-like surfactants.[18] These weakly adsorbed surfactants are displaced from the electrode surface by less negative potentials and are driven by changes in potential-dependent interfacial tension (electrocapillarity). The desorption from Au (111) occurred over a very small potential region, and the readsorption of these insoluble surfactants was found to be complete. A mechanism was proposed to explain these potential-dependent changes based upon electrochemical and spectroelectrochemical studies. These fluorescence results have shown that the reductive desorption of the SAM is very similar and the existence of desorbed molecules near the electrode surface can be explained using the same mechanism developed for the physically adsorbed surfactants. The oxidative readsorption observed for long-chain alkylthiols can be conveniently explained through the existence of these desorbed molecules near the electrode surface.[31]

The fluorescence image of the desorbed fluorescing surfactant at −1.250 V/SCE, shown in Figure 4a, displays significant heterogeneity. A striking correlation can be made between the bottom right of these fluorescence images and a facet observed in a brightfield image of the electrode surface taken before potential cycling (outlined region in Figure 1b). Desorption of the molecules seems to be occurring from particular regions of the Au bead electrode. The images taken while holding at the negative potential limit illustrates the mobility of the desorbed surfactant. Features in the image become less sharp due to a slow diffusion away from the region near the electrode, seen most easily by comparing images B_1, B_2, and B_3. In our previous investigations,[63,64] a decrease in fluorescence intensity for the positive potential scan direction was attributed to readsorption of the surfactant. However, diffusion was not evident in those experiments, and the minimum capacitance did not increase after the negative potential excursion. The decrease in fluorescence intensity observed in this case was mainly attributed to loss of the surfactant from the interface, because the increase in the minimum capacitance indicates incomplete readsorption (via oxidative process) of the surfactant. Also, readsorbed molecules or those adsorbed molecules able to migrate to the desorbed regions would be expected to desorb on the next cycle, and, as we shall demonstrate, regions where fluorescence was observed during this cycle did not fluoresce on subsequent cycles. The hysteresis in the return potential scan can also be explained by the combination of incomplete readsorption and loss of surfactant.

The third potential-imaging cycle was performed with a negative potential limit of −1.300 V/SCE. At this negative potential, the capacitance approached the value of the unmodified electrode surface. After potential cycling, the SAM was significantly perturbed, resulting in a minimum capacitance of 6 μF cm^{-2} and a capacitance scan that begins to resemble the uncoated Au electrode. The fluorescence intensity closely follows the cathodic scan of the previous run, but remains consistently below until reaching the negative potential limit where the maximum in fluorescence intensity became larger. The fluorescence images are similarly heterogeneous as the

previous potential scan, but fluorescence was observed from distinctly different regions of the electrode. The reductively desorbed molecules were also observed to diffuse away from the surface of the electrode shown by the three images at the negative potential limit (E_1, E_2, and E_3). The anodic scan shows a strong decrease in fluorescence in addition to the decrease in capacitance; as before, the incomplete readsorption of the desorbed molecules partially explains the loss of fluorescence intensity, but diffusion away from the electrode plays the main role.

The fourth potential-imaging cycle used a negative potential of −1.350 V/SCE. The capacitance resembles an unmodified electrode interface, indicating a very strong disruption in the adsorbed monolayer. The minimum capacitance in this case was 13 μF cm^{-2}. The corresponding fluorescence intensity was weaker, and the fluorescence image was again not uniform, clearly showing fluorescence in a region that was dark in the previous cycle. Diffusion of the fluorescing molecules was also observed at this potential (H_1, H_2, and H_3).

The potential scan out to −1.400 V/SCE (fifth potential-imaging scan) revealed an electrode surface with a capacitance practically identical to that of the uncoated electrode, and, as expected, no fluorescence was observed. All of the molecules composing the initially complete SAM have been reductively desorbed from the metal surface. Interestingly, at the end of the experiment, fluorescence was observed at the electrolyte surface, strongly suggesting the segregation of the desorbed molecules (now presumably thiolates) to the gas|solution (G|S) interface. An examination of the time lapse fluorescence images in Figure 4 shows that, when reductively desorbed, the molecules stay near the electrode surface and only slowly diffuse away on the time scale of the fluorescence measurements. It is expected that the surfactant would oxidatively readsorb if it remained in the vicinity of the metal surface as in the reductive desorption experiments done on thiols with long alkyl chains. Oxidative readsorption onto bare gold regions would result in fluorescence during the subsequent desorption potential scan. This phenomenon was not observed in these studies, but it could be achieved by using a thiol with a longer alkyl chain, resulting in less solubility in the electrolyte. As the current study demonstrates, there exists a strong similarity between the potential-driven desorption from the electrode surface of covalently attached thiols and of physisorbed lipid-like molecules. Further experiments are planned using a more insoluble fluorescent thiol to confirm that the readsorption process is, like the desorption process, general for both chemisorbed and physisorbed surfactants. One important observation in the current study made clear by our in situ fluorescence imaging is the large-scale heterogeneity in these fluorescence images that was not present in the previous single-crystal studies. The region of the electrode where fluorescence was observed, and therefore where desorption occurred, was strongly influenced by potential and, as we shall show below, electrode surface crystallography or morphology.

3.2. Selective Reductive Desorption. To define in detail the relationship between surface crystallography and desorption potential, image analysis was performed on the first images acquired at each negative potential limit for the second, third, and fourth cycles (negative limits are −1.250, −1.300, and −1.350 V/SCE, respectively), as shown in the first column in Figure 5. Outlines of each image (shown in the second column of each row) were created using a simple segmentation procedure and were overlaid onto the −1.300 V/SCE image, displayed in the third column.

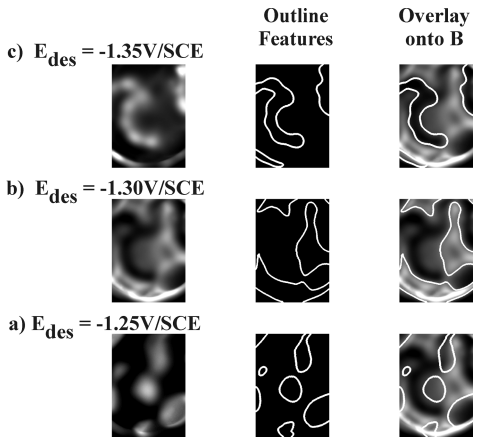

Figure 5. Fluorescence images (first column) obtained at various negative potential limits: (a) −1.250, (b) −1.300, (c) −1.350 V/SCE. Fluorescent regions were outlined (middle column), and then applied to the image recorded at −1.300 V/SCE (last column) to illustrate the regional specificity of the desorption process.

Fluorescence from different regions of the surface is clearly related to the value of the negative potential limit. The small facet observed on the bottom right was desorbed at the least negative potential (−1.250 V/SCE). The image taken at the negative potential limit of the subsequent scan (−1.300 V/SCE) shows no fluorescence from this region, indicating the irreversible loss of the surfactant due to desorption from the facet. The control that potential offers is even clearer when comparing the images taken at −1.350 and −1.300 V/SCE. The fluorescent regions observed for −1.350 V/SCE were not observed to be fluorescent at the other less negative desorption potentials. Conversely, all regions would show fluorescence if the desorption potential limit is pushed to −1.350 V/SCE on the first cycle.

The sensitivity toward the value of the potential driving these changes is clear and can be understood in terms of the energetics of the electrode/electrolyte interface. Bead electrodes are typically composed of regions of differing surface crystallography,[75] which can be visualized by etching in aqua regia. The SEM and optical image (Figure 6a and b, respectively) of the etched Au bead show the heterogeneity of our electrode surface with some features outlined in Figure 6c. Because the bead electrode was not a single crystal, the presence of grain boundaries and defects can be used in comparing the fluorescence images with the electrode surface morphology. The SEM and optical image clearly show the facet (labeled I), also observed in the brightfield image shown in Figure 1b. In this region, fluorescence was observed for the least negative desorption potential. Because studies of reductive desorption of thiol SAMs on Au single crystals have shown the dependence of reductive desorption potential on surface crystallography, we anticipate that the regions first desorbed were from surfaces with a (111) orientation. This was confirmed for the facet on the bottom right (I) by EBSD.

Desorption from other regions of the electrode surface are most likely also dependent on surface crystallography, but EBSD

(75) Perdriel, C. L.; Arvia, A. J.; Ipohorski, M. *J. Electroanal. Chem. Interfacial Electrochem.* **1986**, *215*, 317−329.

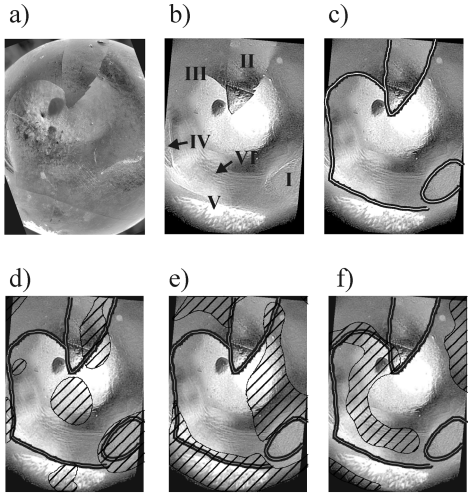

Figure 6. Correlation between surface morphology (revealed through etching) and fluorescence features at increasingly negative potentials. (a) SEM image of etched electrode; (b) brightfield image with labeled features; and (c) brightfield image with features outlined. Outlined brightfield image with masks created from (d) −1.250, (e) −1.300, and (f) −1.350 V/SCE fluorescence images.

was unable to unambiguously determine the surface normals for curved portions of the surface or for regions that did not exhibit clear facets. Smooth reflective features at the top of the image resembling an elongated triangle (labeled II) with a small circular region on its left are obvious. Starting from the triangular region, a grain boundary (labeled III) curves off to the left and then downward toward another half-moon feature (labeled IV). This boundary continues on the bottom of the image toward the facet on the right (labeled V). These key features allow overlaying of the fluorescence images with the optical image. This was accomplished by starting with the facet (I) and overlaying the first desorption image using the oblong shape of the facet in orienting the optical image. We are confident in our analysis because SEM images of the complete bead surface did not reveal any other large oblong facet. This optical image of the electrode was created by overlaying the in-focus regions from a number of pictures with differing focal planes to facilitate comparison with the SEM image. This was not done for the fluorescence images. Fluorescence will be measured from regions not in the focal plane, so a direct comparison is qualitative but still very useful.

Figure 6d shows the mask created from the fluorescence image recorded at −1.250 V/SCE overlaid on the outlined optical image of the electrode. The optical image was rotated to optimally fit the shape of the facet. The fluorescent feature protruding from the center top matches well with the extended triangular feature on the optical image (II). Unfortunately, the feature in the center of the image does not seem to correlate well with any surface irregularities. Overlaying the mask created from the −1.300 V/SCE is shown in Figure 6e. The facet is no longer fluorescent, but the regions immediately around the facet are fluorescent, allowing a clear fit with the optical image. The grain boundary on the bottom of the image (V) correlates with the observed fluorescence. The region outlined at the top left also correlates well with the area outlined by the grain boundaries that extend from the triangular region to the left. The fluorescence observed on the right-hand side is constrained between the facet and the grain boundary outlining region II. Finally, overlaying of the mask created from the −1.350 V/SCE image is shown in Figure 6f. The curved region outlined correlates well with the lines that decorate the electrode surface (labeled VI). The small circular region next to the triangular feature is encompassed in the outlined area, and the grain boundary that curves off to the left from the triangular region (III) and (V) is also captured in the outlined region.

Overall, the correlation of the fluorescence features to the electrode surface features is quite close, and, although an exact correspondence of fluorescence to surface features was not possible, a number of regions of fluorescence were "assigned" to surface features. The potential-dependent fluorescence features seem to match well with the electrode surface structure from which desorption took place.

4. Conclusions

The reductive desorption of a SAM was monitored for the first time with electrofluorescence microscopy, and the fate of the desorbed molecules was determined. This union of electrochemical techniques and spatially resolved fluorescence has proven to be a powerful and nondestructive method of monitoring the potential-induced changes in adsorbed organic layers. We have shown the reductive desorption of a SAM of a slightly soluble fluorescent thiol from selective regions of a polycrystalline Au bead. The observation of intense fluorescence at negative potentials displays the desorption of the surfactant from the metal surface. The slight disruption of this desorbed layer was observed through both capacitive measurements and diffusion of the thiol. A fluorescence increase at desorption has been observed in the case of physically adsorbed surfactants and is strikingly similar to the desorption process for these covalently bound molecules. This implies that the mechanism of desorption is general and may hold for other systems as well. The readsorption process of thiols may have the same generality if a less soluble thiol is used; however, the slight solubility of the surfactant in this experiment had the unique advantage of allowing selective exposure of different regions of the electrode through control of the potential. This selective desorption was further defined using the techniques of EBSD with the conclusive assignment of desorption from the (111) facet at −1.250 V/SCE. Furthermore, image-masking techniques led to the assignment of desorption from areas of the electrode surface where EBSD was unable to unambiguously assign a crystal face. This selective desorption may have profound application in the creation of a thiol-modified surface with a desired pattern and multifunction, and in the electrofluorescence technique in the detection strategy used for SAM array sensors.

Acknowledgment. This work was supported by the NSERC (Canada). J.L.S. was supported by a NSERC PGS B graduate student fellowship.

Supporting Information Available: Synthesis of 4,4-difluoro-1,3,5,7-tetramethyl-8-[(10-mercapto)]-4-bora-3a,4a-diaza-*s*-indacene (BodipyC10SH). This material is available free of charge via the Internet at http://pubs.acs.org.

JA0494095